Journal of Geophysical Research: Earth Surface

RESEARCH ARTICLE
10.1029/2017JF004540

Key Points:
- The imprint of biogeomorphic processes on salt marsh drainage network sinuosity during the pioneer stages is *inherited* by later successional vegetation types
- Vegetation patch-size distributions in salt marsh vegetations from the pioneer to late successional stages correspond to power laws, suggesting the presence of self-organizational processes
- Vegetation patch size in salt marshes shows an inverse logarithmic relationship with tidal channel sinuosity, irrespective of vegetation type and elevation

Correspondence to:
A. Taramelli,
andrea.taramelli@isprambiente.it

Citation:
Taramelli, A., Valentini, E., Cornacchia, L., Monbaliu, J., & Sabbe, K. (2018). Indications of dynamic effects on scaling relationships between channel sinuosity and vegetation patch size across a salt marsh platform. *Journal of Geophysical Research: Earth Surface*, *123*, 2714–2731. https://doi.org/10.1029/2017JF004540

Received 3 NOV 2017
Accepted 8 SEP 2018
Accepted article online 19 SEP 2018
Published online 29 OCT 2018

Indications of Dynamic Effects on Scaling Relationships Between Channel Sinuosity and Vegetation Patch Size Across a Salt Marsh Platform

Andrea Taramelli[1,2], Emiliana Valentini[1], Loreta Cornacchia[1,3], Jaak Monbaliu[4], and Koen Sabbe[5]

[1]ISPRA (Institute for Environmental Protection and Research), Rome, Italy, [2]IUSS University School for Advanced Study of Pavia, Pavia, Italy, [3]NIOZ Royal Netherlands Institute for Sea Research, Department of Estuarine and Delta Systems, Utrecht University, Yerseke, Netherlands, [4]Hydraulics Laboratory, Department of Civil Engineering, Katholieke Universiteit Leuven, Leuven, Belgium, [5]Laboratory of Protistology and Aquatic Ecology, Department of Biology, Ghent University, Ghent, Belgium

Abstract Salt marshes are important coastal areas that consist of a vegetated intertidal marsh platform and a drainage network of tidal channels. How salt marshes and their drainage networks develop is not fully understood, but it has been shown that the biogeomorphic interactions and feedbacks between vegetation development and channel formation play an important role. We examined the relationships among tidal channel sinuosity, marsh roughness, vegetation type (pioneer, *Elymus athericus* or *Phragmites australis*), and patch size at different spatial scales using a high-resolution vegetation map (derived from aerial photography) and lower-resolution satellite imagery processed with linear spectral mixture analysis. The patch-size distribution in all vegetation types corresponded to a power law, suggesting the presence of self-organizational processes. While small vegetation patches are more dominant in pioneer vegetation, they were present in all vegetation types. The largest patch size is restricted to *E. athericus*. We observed an inverse logarithmic relationship between channel sinuosity and vegetation patch size in all vegetation types. The fact that this relationship is observed in both pioneer and later successional stages suggests that after the establishment of a drainage network in the dynamic pioneer stages of salt marsh development, the later stages of salt marsh succession largely inherit the meandering pattern of the early successional stages. Our study confirms recent evidence that no significant changes in the specific features of tidal channel networks (e.g., channel width, drainage density, and efficiency) take place during the later stages of salt marsh development.

1. Introduction

Coastal transitional environments are highly dynamic and complex systems. This complexity is particularly evident in salt marshes, which are natural landforms shaped by the interactions among hydrodynamic forces, sediment input, and vegetation (Temmerman et al., 2007). Salt marshes represent one of the most important types of coastal wetlands, both for their ecological value and for their coastal defense characteristics (Adam, 1990; Kirwan et al., 2016; Yapp et al., 1916, 1917). Salt marshes can be divided into three characteristic components based on their elevation: (i) a tidal flat of unvegetated sediment, usually lying below the mean high water level; (ii) a marsh platform colonized by halophytic vegetation and located at the transition between the emerged and submerged environments; and (iii) a drainage channel network that breaks up the vegetated surface and controls tidal flow in and out of the marsh, hence controlling exchanges between the marsh interior and exterior. These three zones interact on different scales, resulting in the formation of highly intricate patterns of vegetated areas and tidal channel systems (Bouma et al., 2009).

Salt marshes display a high degree of heterogeneity at multiple spatial scales, which is caused by different internal and external forces; specifically, sea level and tides are the most important external stress factors, while the dominant internal force is the halophytic vegetation itself (Allen, 2000). Strong interactions between vegetation and physical forces shape salt marsh initiation and development (Beeftink, 1966; Boon, 1975; Boon & Byrne, 1981; Bouma et al., 2009; French & Stoddart, 1992; Novakowski et al., 2004; Pethick, 1980; van Wesenbeeck et al., 2008), the hydrodynamics of salt marsh channels (Fagherazzi et al., 2008; Temmerman, 2005), and their morphometric features (Fagherazzi et al., 2004, 2012; French, 1993, 2006; Marani et al., 2003, 2006; Rinaldo et al., 1999a, 1999b). Although modeling studies have enhanced

our knowledge about the long-term biomorphodynamic evolution of intertidal areas and salt marshes in particular (D'Alpaos, Lanzoni, Marani, Fagherazzi, Rinaldo, 2005; D'Alpaos et al., 2006; Fagherazzi & Furbish, 2001; Fagherazzi & Sun, 2004), comparatively little empirical knowledge is available on the evolution of salt marshes in response to changes in intertidal vegetation and platform elevation (D'Alpaos et al., 2007, 2006; Defina et al., 2007; Fagherazzi et al., 2006); moreover, there is particularly limited information available on the transition dynamics during the establishment of channel sinuosity in relation to the main patterns of spatial vegetation (Foti & Ramírez, 2013; Temmerman et al., 2007; Vandenbruwaene et al., 2012). During the initial stages of salt marsh development (i.e., from the unvegetated tidal flat to the vegetated stage), the establishment of vegetation can have both erosional and stabilizing effects (Friedrichs, 1995; Friedrichs & Aubrey, 1988). The importance of these effects depends on the channel incision and slope. If channels were already formed in the unvegetated mudflat stage, then vegetation will mainly have a stabilizing effect. However, if channels are not yet fully formed, biological-physical feedbacks (Bouma et al., 2016; Corenblit et al., 2015; Hu et al., 2015) between vegetation tussocks (e.g., the pioneer *Spartina*) and sediment will enhance erosion and, hence, channel incision between the vegetation patches (Bouma et al., 2007; Schwarz et al., 2014, 2015; Vandenbruwaene et al., 2011; van Wesenbeeck et al., 2008). Either way, once vegetation is established, an increase in channel branching and meandering is observed (Pestrong, 1965), which results in increased channel drainage density (Temmerman et al., 2007; Vandenbruwaene et al., 2012) and efficiency (Kearney & Fagherazzi, 2016). Sediment trapping by the pioneer vegetation will lead to an increase in sediment stability and elevation, which enables the later successional vegetation stages to colonize (D'Alpaos, Lanzoni, Marani, Bonometto, et al., 2005). At the same time, smaller patches can begin merging into larger patches; over time, this process will lead to the formation of a marsh platform that is dissected by major channels, as has been observed in studies using aerial photography and remote sensing (RS) approaches (Temmerman et al., 2007; Vandenbruwaene et al., 2011; Wang & Temmerman, 2013). Currently, it is not completely clear what happens to the geometry of the drainage networks in these later stages of salt marsh development (Maréchal et al., 2012; Mariotti & Fagherazzi, 2010). Modeling approaches suggest that after vegetation has established, further planimetric network evolution is mainly characterized by meander formation and evolution (D'Alpaos et al., 2007; Schwarz et al., 2014); however, empirical work has shown that, after vegetation establishment and patch-size growth, the presence of vegetation will *freeze* the structure of the channel network (as evidenced by, e.g., no further changes in channel density and channel width; Vandenbruwaene et al., 2012). Studies on fluvial systems and megadeltas (Passalacqua et al., 2013; Perron & Fagherazzi, 2012) have highlighted that plants established on freshly deposited areas of a braidplain during low flow had the effect of progressively focusing the high flow so that a single dominant channel developed over a wide range of spatial scales (Fagherazzi, 2008; Garofalo, 1980). Further changes in channel geometry and, more specifically, sinuosity are then mainly related to changes in flow resistance caused by changes in topography and/or vegetation abundance; moreover, denser vegetation leads to increases in sinuosity as long as the slope remains constant (Lazarus & Constantine, 2013). Likewise, it has been hypothesized that higher vegetation abundance in salt marshes will lead to increased channel density (Temmerman et al., 2007).

To date, the relationships among the vegetation successional stage, vegetation patch size, and sinuosity have not been thoroughly explored in salt marshes. More specifically, it is not known how vegetation patch size is distributed from the early-stage pioneer zone to the later successional stages in the high marsh platform; it is also unclear how patch size is related to sinuosity.

To this end, most RS studies have focused on detecting spatial patterns through the use of aerial sensors (e.g., Ibrahim & Monbaliu, 2011; Temmerman et al., 2007; van de Koppel et al., 2005) and lower-resolution images (Frazier & Page, 2000; Taramelli et al., 2017). However, the use of spatial variables derived from RS imagery offers an ideal tool to study the relationships among vegetation type, patch-size distribution, and channel sinuosity (Jefferies et al., 2006; Méléder et al., 2010; Moffett et al., 2015; Vande Castle, 1998; Wang et al., 2007). In fact, to capture smaller-scale variation, linear spectral mixture analysis (LSMA) allows the consideration of subpixel variation (Manzo et al., 2014; Valentini et al., 2014) and provides a validated tool that can be used to study temporal multiscale channel and vegetation variability in tidal ecosystems (Taramelli et al., 2017; Taramelli, Valentini, et al., 2014).

In the present study, we examine the relationships between vegetation patch size and channel sinuosity in a salt marsh in the Netherlands. We hypothesized that as the marsh matures from pioneer to later stages, sinuosity will increase because the denser vegetation (i.e., the later successional stages) would increase flow

resistance. We used a combination of RS observations to investigate whether the same relationships hold at different spatial scales (Sousa & Small, 2017; Van Belzen, 2011), including a high-resolution vegetation map based on aerial photography and medium-resolution RS data (SPOT, Satellite Pour l'Observation de la Terre), to characterize vegetation by applying the LSMA and to extract the channel sinuosity for the optical RS images (Frazier & Page, 2000; Mason et al., 2006).

This paper is organized as follows. The first part of section 2 introduces the study area and discusses the field and the Earth observation data used. The LSMA, which considers subpixel variation, and its main ecological and physical assumptions (e.g., vegetation patches and sinuosity) are discussed in the second part of section 2. Section 3 presents and discusses the main results obtained by applying the power law conceptual model for explaining why annealing patches are merging across salt marshes, which are then inherited in a later stage. Finally, a set of conclusions close the paper.

2. Study Area

The study area is located in the Scheldt estuary (Figure 1) in the Netherlands, specifically in a catchment area that covers one of the most densely populated regions in Europe, with a total of 10 million people (Meire et al., 2005). The river Scheldt originates in northern France and flows through Belgium and the Netherlands into the North Sea, with a total length of 355 km (Meire et al., 2005). The Scheldt estuary (Baeyens et al., 1997) has a mesotidal to macrotidal regime across the entire estuary (up to Ghent). The tidal excursion is variable within the estuary. At the mouth, the average tidal range is 3.8 m (between 2.81 m at neap tide and 4.85 m at spring tide).

The study site, which is called the *Verdronken Land van Saeftinghe*, is a nature reserve located in the brackish (oligohaline) section. Saeftinghe is the largest salt marsh in the estuary (approximately 30 km^2) and ranks among the largest in Europe. The average tidal range at the site is 4.88 m (Vandenbruwaene et al., 2012). In the 1930s, only 25% of the area was covered by salt marsh vegetation, while the rest of the area consisted of mudflats and tidal channels (Vandenbruwaene et al., 2012). Today, the proportions are reversed: Saeftinghe consists of 30% mudflats and channel systems, while the remaining 70% of the surface is covered by salt marsh vegetation. In Saeftinghe, climax stands of common reed (*Phragmites australis*) can be found. Sea couch (*Elymus athericus*), an upper-marsh species with a highly competitive capacity for nitrogen assimilation, is the dominant grass species. The pioneer zone is mainly colonized by patches of *Spartina*.

3. Materials and Methods

3.1. Available Data

3.1.1. High-Resolution Vegetation Map and Digital Terrain Model

We used a vegetation map and a digital terrain model (DTM), both of which were acquired in 2010, to characterize the vegetation (e.g., typology and spatial distribution) and the geomorphic characteristics of the study site (e.g., marsh elevation and tidal channel sinuosity). The vegetation map of the western Scheldt salt marshes was provided by Rijkswaterstaat (hereafter RWS; part of the Dutch Ministry of Infrastructure and the Environment) and is available upon request from the RWS Servicedesk Data (http://www.rijkswaterstaat.nl/water/waterbeheer/natuur-en-milieu/ecotopen/meer-weten/index.aspx). The data set was obtained through stereoscopic interpretation of false-color aerial images at a 1:50,000 scale through the use of a digital photogrammetric system. The vegetation mapping was performed according to the landscape-guided and photo-guided methods (Tiner, 2016). This method is a variant of the landscape-guided method and is generally used when the complete area can be visited in the field (Janssen, 2001). In both methodologies, the interpretation was also supported by fieldwork, and finally, the maps were digitized and stored in a geographical information system, GIS (Tolman & Pranger, 2012).

The RWS vegetation map was integrated with the DTM of 2010, which was obtained from a light detection and ranging (LiDAR) survey (2 × 2-m spatial resolution and a maximum vertical error of ±0.05 m) and provided by RWS. The elevation DTM was also used to determine the elevation range of the different vegetation types (see end of section 3.2) and to improve the vegetation classification of the satellite imagery (see RS data set below).

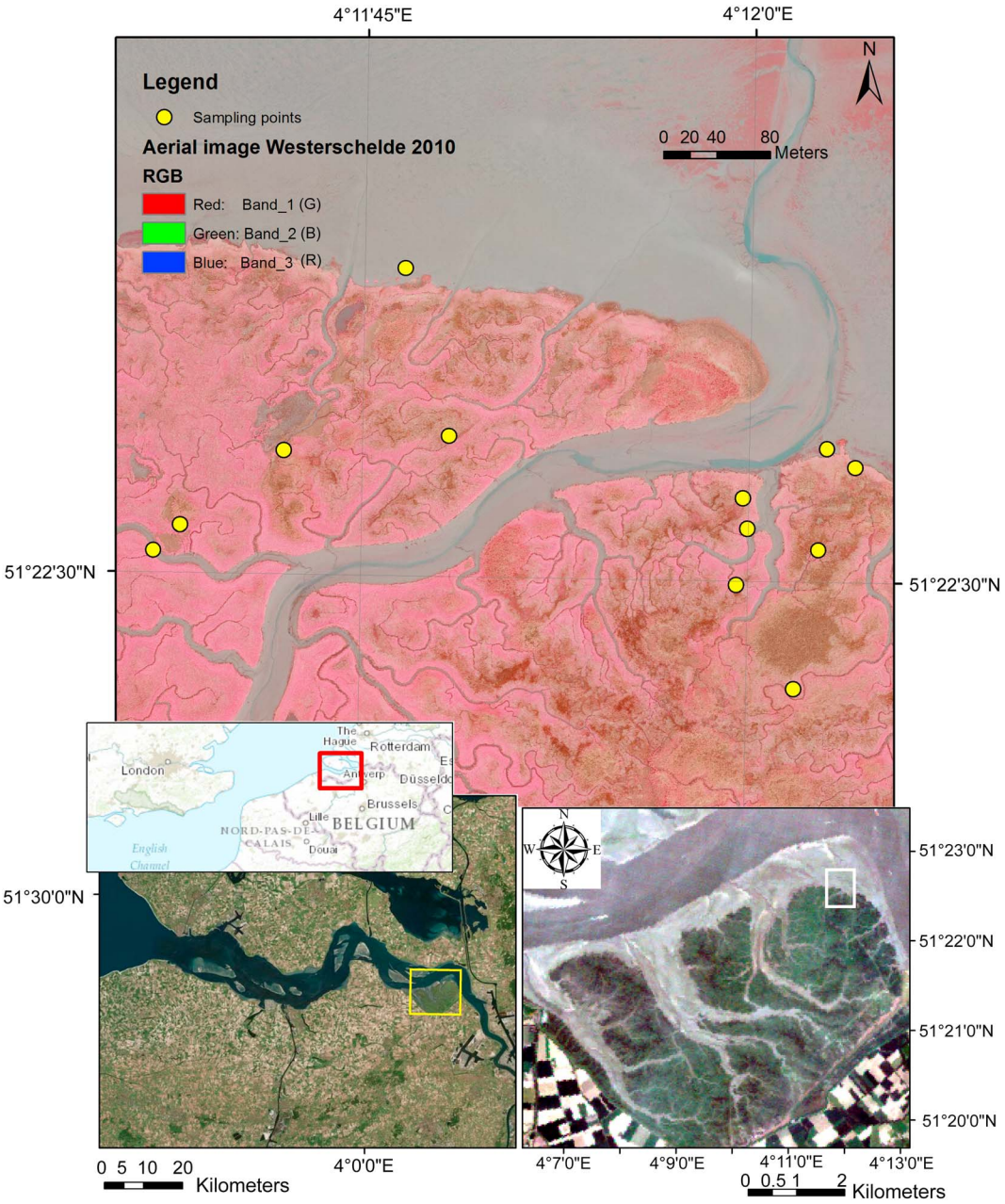

Figure 1. (top) False color aerial image of the salt marsh and location of sampling points of spectroradiometric measurements. Landsat satellite image of the Scheldt estuary (bottom left), close up of the Saeftinghe salt marsh (bottom right), and the Scheldt estuary location in the northern part of Europe (top right).

3.1.2. Lower-Resolution Satellite Imagery (SPOT)

To test the effects of the decreasing spatial resolution on the relationships between vegetation and geomorphic features, we also analyzed lower-resolution RS images taken during low tide for two different time points in 1999 and 2012. For 1999, we used an archived SPOT-4 satellite image (Spot Image, 2002), while the 2012 image was acquired through a SPOT-4 overpass of the Saeftinghe salt marsh (Table 1) during the field campaign (see below). The satellite carries the High-Resolution Visible and Infrared optical sensor, which measures the radiance of the Earth's surface in three bands in the visible-near infrared and one in the middle infrared, with a ground resolution of 20 m. The High-Resolution Visible and Infrared sensor characteristics and details on the overpass are described in Table 1, as is the tidal level for the reference station of Bath (The Netherlands).

Table 1
Characteristics of the SPOT4 HRVIR Sensor (Spot Image, 2002), the Archived Image (1999) and Overpass Details (2012 Campaign), and the DTM (2010) Used in This Study

	1999	2012	Digital terrain model (DTM) 2010
Platform	SPOT-4 Satellite	SPOT-4 Satellite	Airborne LiDAR
Spatial resolution (m)	20 × 20	20 × 20	2 × 2
Spectral range (nm)	500–1750	500–1750	n/a
Bands	4	4	1
Acquisition date	1 May 1999	4 July 2012	25–28–29 April 2010 14/05/2010
Flight time (ECT)	11:03	10:30	n/a
Tidal level	−2.14 m	−2.23 m (Normal Amsterdam Level)	n/a

Note. HRVIR = High-Resolution Visible and Infrared; LiDAR = light detection and ranging; SPOT-4 = Satellite Pour l'Observation de la Terre 4; ECT = European Connoisseurs Travel.

The SPOT images were preprocessed for radiometric correction first by a transformation to at-sensor radiances using gain and offset information, and then to at-sensor reflectance to compensate for variations in the illumination conditions and solar irradiance (Chander & Markham, 2003). After the radiometric corrections, the images were georeferenced into a standard map projection (Universal Transverse Mercator datum WGS 1984) and georeferenced through a set of ground control points that were selected based on a reference Landsat image (30-m resolution).

3.1.3. In Situ Field Observations: Spectroradiometric Measurements of Macrophytes

Field observations (macrophytes and spectroradiometric measurements) were carried out simultaneously with the SPOT RS acquisition of 2012. The total extent of the study area (30 km^2) made a detailed analysis of the distribution of vegetation and sediment for the entire site impossible. For this reason, we used the preliminary analysis of the 1999 SPOT image to identify a subarea (Figure 1, top) that represented the full range of the vegetation type and drainage heterogeneity of the area as much as possible.

A total of 12 stations were sampled on the salt marsh in the subarea (Figure 1). We focused on three main vegetation types that were taxonomically and structurally uniform: the pioneer and low-vegetation zone (vegetation height: 0–30 cm) that was mainly colonized by *Spartina*, the high vegetation zone (30–100 cm) that was colonized by *E. athericus*, and the high vegetation zone that was dominated by stands (> 1 m) of *P. australis*. For each sampling station, the coordinates were collected using a Trimble® GeoXT™ handheld Global Positioning System. At each sampling site, the vegetation presence/absence was recorded together with the identification of the dominant plant species and its maximum height. The spectral signature of the vegetation was acquired for every sampling station using an Analytical Spectral Devices Hi-Res Fieldspec® 3 portable spectroradiometer. For each station, first a white reference spectrum of the Spectralon panel mounted on a tripod was acquired at a distance of 15 cm, and then 10 subsequent spectra of the same target from a distance of 1 m were collected to account for measurement errors and variability. The 10 spectra were then averaged to obtain a single spectrum for each station.

3.2. Spectral Mixing Analysis

The first processing step for both of the calibrated SPOT images was LSMA. SMA is a commonly used technique used to obtain quantitative results at subpixel resolution since it can provide information on the abundance of surface components inside the fundamental elements constituting the image (Boardman, 1993) without assigning each pixel to a single class as is done in *hard* classifications (Taramelli & Melelli, 2009). Therefore, this method represents one of the most suitable processing techniques for heterogeneous environments.

The methodology is based on the fact that within pixels, the spectral signature of a pure pixel represents a fundamental physical component (e.g., water) and not a mixed signal that results from a mixture of components (Adams et al., 1986; Johnson et al., 1983; Smith et al., 1985). The technique allows the determination of mixed fractions within each pixel based on the identification of pure spectra, also called end-members, that mix with each other and give rise to the spectral response of each surface element

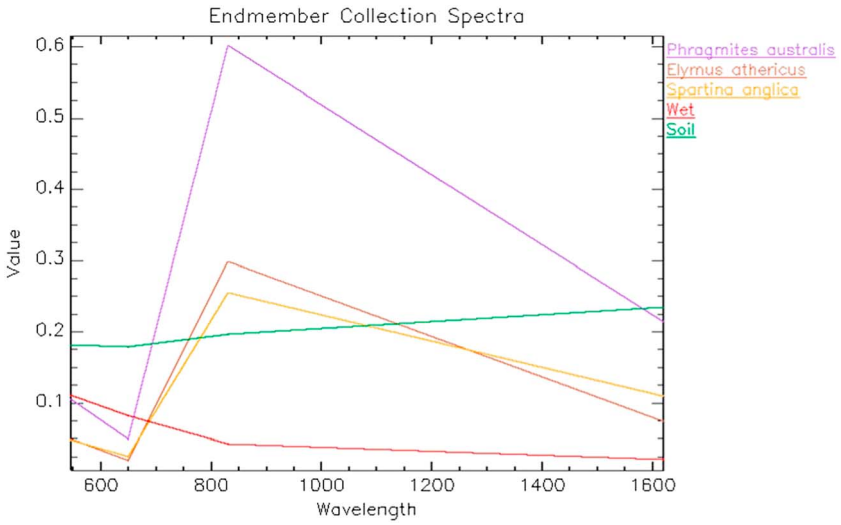

Figure 2. Spectral signatures of the five end-members selected for the spectral mixing analysis in the Saeftinghe salt marsh.

in the scene. The results are fraction estimates of end-member abundance at the subpixel scale, on the basis of the pure spectra found in the image. The image will then be represented by a spatially continuous map of fractional abundance for each physical surface component (Adams et al., 1986; Small, 2004; Smith et al., 1985).

End-member selection first involves determining the mixing space topology and structure through principal component analysis and then determining the dimensionality and linearity to select spectral end-members. The choice of the end-members is made on the basis of a 2-D scatterplot between the first three principal components of the multispectral image. Pure spectra are located at the apexes of the mixing space.

Prior to image processing, a mask was created for the area of interest based on the boundaries of the Saeftinghe Nature Reserve. This step was performed to exclude anthropogenic and agricultural areas from the spectral unmixing and from the analysis of vegetation spatial patterns. We then processed the image using two different linear unmixing models. More specifically, we applied (a) a linear three-end-member model (vegetation, soil and wet) (Taramelli, DiMatteo, et al., 2014; Valentini et al., 2014) to identify the channel network and the vegetated marsh platform as a whole, and (b) a linear five-end-member model (pioneer vegetation (*Spartina anglica*), *E. athericus*, reed stands (*P. australis*), soil and wet) to map—in detail—the typology of the vegetation cover (see Figure 2 for the spectral signatures of the five end-members). The soil and wet end-members were extracted from the mixing space of the image, and by using RGB for substrate (S), vegetation (V), and dark (D), respectively, the vegetation areas that were in contrast with the low-albedo soil substrates (including channels) were identified. The three vegetation end-members (*S. anglica*, *E. athericus*, and *P. australis*) were imported from the field spectral library. The final classification used both field and image spectral libraries and shows the fractional composites for the Saefthinghe salt marsh that are generated by assigning three end-members to the red, green, and blue layers of both SPOT images (Taramelli, Pasqui, et al., 2013). Thus, the final vegetation classification map is a continuous variable that corresponds to the green vegetation fraction covering a unit of ground area as seen from the nadir direction (Filipponi et al., 2018). It depends on the canopy and gives information about the vegetation pixel purity representing the quantitative measurements of the physical properties and abundance of vegetation. The measurements yield quantitative estimates of the areal abundance (named the fractional cover) within each pixel of the vegetation cover that is identified by the selected end-members.

We then built and implemented a decision tree classification algorithm that classified each pixel based on the abundance categories from fractions of cover typologies and named each pixel based on the strongest Pearson correlation between the selected spectral profiles and the field spectral library (Manzo et al., 2014; Valentini et al., 2014). Every pixel in the image was assigned to a certain class using a threshold value in

Table 2
Confusion Matrix for SPOT Classification of the Saeftinghe Salt Marsh, Expressed as the Percentage of Correctly Classified Pixels in Each Class

	Ground truth: RWS 2010 vegetation map (percent)			
Classes	Pioneer vegetation	Climax *Elymus athericus*	Climax reed	Total
Pioneer vegetation	**60.37**	38.46	1.17	100
Elymus athericus	4.13	**94.85**	1.02	100
Reed	0.56	39.56	**59.89**	100

Note. Overall accuracy (irrespective of classes): 90.8%, *K* coefficient: 0.56. The diagonal bold values are the average classification rate. SPOT = Satellite Pour l'Observation de la Terre.

fractional cover (i.e., ≥ 0.5552 for the wet class; ≥ 0.5950 for the soil class; ≥ 0.4992 for *P. australis*; ≥ 0.5507 for *E. athericus*; and ≥ 0.8945 for pioneer vegetation). The LiDAR elevation ranges for each vegetation type, which were obtained from the RWS vegetation map, were used to determine the vegetation class for the pixels where the threshold was not reached and, therefore, could not be classified (Taramelli & Melelli, 2009; Taramelli, Pasqui, et al., 2013). These pixels were classified by performing principal component analysis between the three fraction maps and the elevation value of the LiDAR survey provided by RWS based on information on the distribution of vegetation classes in the LIDAR-elevation range value (Hladik et al., 2013; Taramelli, Valentini, et al., 2013). The method reassigned classes using these elevation ranges within the mixing space and resulted in a final overall classification accuracy of 90% between the SPOT 2012 image classification and the RWS vegetation map of the Saeftinghe salt marsh from 2010 (cf. above). Both class-by-class accuracy and overall accuracy were computed to identify the proportion of correctly classified pixels with respect to the total pixels in the class and the overall mapping accuracy (see Section 4.1 and Table 2). The final results were two classification maps, one for 1999 and one for 2012.

3.3. Mapping Vegetation Patches

The spatial vegetation structure was characterized as the size-frequency distribution of the vegetation patches (the number of contiguous pixels showing the same typology of vegetation), with patches that occur at sizes within the pixel resolution of SPOT imagery (20 × 20 m), defined as the areas that maintained homogeneity with respect to a quantitative radiometric measurement (Forster & Jesus, 2006; Silvestri et al., 2002, 2003; Small, 2004), such as those in the pioneer zone. The second step was to define the boundaries of each pattern based on the binary image for each class. Patterns were delimited using the von Neumann neighborhood algorithm (von Neumann, 1951). Patch boundaries were defined based on the connectivity of each vegetation pixel to its four neighboring (i.e., adjacent) pixels. The area (number of pixels) was calculated for each patch. Raster maps of vegetation patterns were imported into GIS software (ArcMap 10.0) and converted into a polygonal shapefile to create a layer that was complementary to channel sinuosity.

3.4. Patch-Size Distribution

Based on the vegetation patterns defined in the previous step, we calculated the size-frequency distribution of patch size, and we investigated whether the relationship could be described by a power law to detect the presence of scale-invariant patterns (Newman, 2005). A power law distribution of patch sizes can be interpreted as a sign of self-organization (Rietkerk & van de Koppel, 2008; Scanlon et al., 2007; Schoelynck et al., 2012; Small & Sousa, 2016). A typical power law distribution can be described as a cumulative distribution indicating the probability $P(X \geq x)$ that a patch-size X is larger than or equal to x. In this case, the power law is of the following form:

$$P(X \geq x) \propto x^{-\alpha} \tag{1}$$

where x is the patch size, and α is the scaling exponent of the distribution (Clauset et al., 2009).

In particular, we were interested in understanding whether the spatial structure of the vegetation patches carried any signature of the processes responsible for marsh formation and evolution and whether a statistical analysis of vegetation metrics highlighted the scaling breaks and the characteristic scales of marsh-forming processes (Taramelli et al., 2015; Temmerman et al., 2007; van de Koppel et al., 2005).

We fitted the power law to the data using the methods of Clauset et al. (2009), through which we estimated α and the lower limit of the observed power law behavior, x_{min}, using the method of maximum likelihood, which uses the scaling parameter for both the discrete and the continuous cases and is derived from the width. The hypothesis is then tested using the Kolmogorov-Smirnov (KS) statistic for the goodness of fit between the empirical data and a large number of synthetic data sets; the latter is sampled from a true power law distribution using the same scaling parameter α and lower limit x_{min} of the distribution that best fit the empirical data. Each synthetic data set is then fitted to its own power law model, and the KS statistic is calculated for each case considering the best fit power law for that data set—and not for the original distribution from which the sample was drawn. This generates a *p* value that quantifies the plausibility of the hypothesis: if greater than 0.1, then the power law is plausible for the data since the actual KS statistic is better than that of 10% of those generated for the synthetic distributions.

3.5. Channel Network Characterization

The geomorphological characterization was based on the calculation of channel geometric properties, more specifically, channel sinuosity. From the DTM of 2010 provided by RWS, we extracted the channel network using literature algorithms (Fagherazzi et al., 1999; Taramelli et al., 2008), as explained below. From the SPOT images, the channel network was extracted from fraction maps using the same methods as those used for marsh vegetation patterns; however, in this case, the processing started from the *wet* end-member.

Once the SPOT images were exoatmospherically corrected, the Substrate Vegetation Dark (SVD) end-member fractions and field work radiometry were used to spectrally unmix the scenes (Valentini et al., 2014). As in Small (2004), a unit sum constraint was applied. At this stage, the channel fraction maps were converted into presence/absence images based on a threshold fraction value that was estimated using *wet*/*dark* and vegetation end-members after a linear dark shadow function was removed (Small & Sohn, 2015; Taramelli & Melelli, 2009). To build and implement the final classification algorithm, we applied a linear function of wavelength λ as a result of the upward curvature of the bottom of the distribution (i.e., the lowest dark fraction at each illumination value) in the mixing space, where 1 corresponds to channel and 0 to marsh vegetation (Mason et al., 2006). To address the dark end-member fraction component related to illumination, the linear trend between the incidence angle and the dark fraction should be minimized, and this process was achieved using a pixel-by-pixel correction equation with an illumination function solving for the slope value that minimized the correlation between the dark end-member fraction and the incidence angle. Since a unit sum constraint was applied, the fraction added or removed from the dark end-member was distributed proportionally to the dark and vegetation end-members, which allowed for a match between the coarse-scale vegetation analysis and a comparably coarse channel network (Small & Milesi, 2013).

In both SPOT images, the reclassified image was imported in MATLAB for network extraction using the skeletonization algorithm (Gonzalez et al., 2004). This morphological operation is used on binary images to reduce each pixel element of the channel network to the thickness of a single row of pixels and to obtain the object's skeleton while still preserving the original shape and connectivity. The algorithm from Gonzalez et al. (2004) was repeated until further reiterations did not impose any changes on the skeleton structure. Linear and short segments were not considered in the analysis (Figure 3a).

The degree of meandering of the channel network was then measured quantitatively through the calculation of channel sinuosity. Sinuosity was calculated as the ratio $s = l/L$ between the along-stream length l to the straight-line distance L between the starting and ending points (i.e., the two nodes of each channel; Barbour, 2008; Stark et al., 2010; Taramelli & Barbour, 2006). Branch points (points of channel bifurcation) were detected and subtracted from the channel network skeleton to obtain isolated branches. We calculated the along-path distance l for each skeletonized branch and the straight-line distance L between its endpoints.

As a final elaboration in the attempt to evaluate the morphometric relationship between sinuosity and floodplain roughness relative to slope in respect to vegetation, we used the calculation of the ratio of roughness (R) to slope (S; Lazarus & Constantine, 2013). The slope was obtained from the DTM and calculated, for each cell, as the maximum rate of variation of the dimension value of a pixel compared to its eight adjacent cells. The maximum variation of elevation over the distance between the reference cell and its eight neighbors identifies the slope value. The slope was then averaged within the cells forming a vegetation patch so that the value could be related to the sinuosity value of the channel bounding that patch. Roughness was

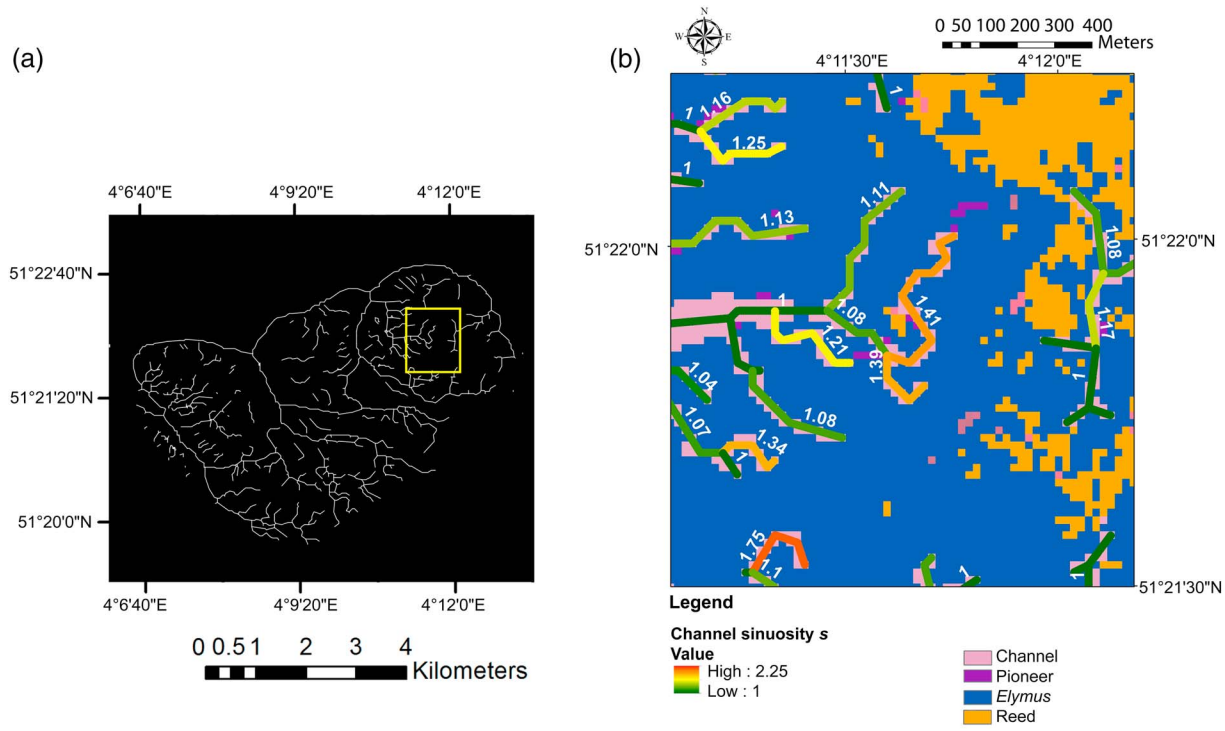

Figure 3. (a) Total channel network; (b) detail of vegetation mapping classification and computed channel sinuosity (numbers in white) for the SPOT-4 image of 2012. SPOT-4 = Satellite Pour l'Observation de la Terre 4.

calculated from the DTM as the standard deviation of elevation within each vegetation patch. This index is useful as a measure of topographic variability and is used to characterize landscape features.

3.6. Relationship Between Vegetation and Sinuosity

To calculate the relationship between vegetation patches and channel sinuosity, we performed a spatial analysis in which patches were associated with the channels that bounded them, both on the RWS vegetation map (DTM [2010]) and on the SPOT images (1999 and 2012). To perform this analysis on the SPOT images, we employed the classification map where the vegetated marsh is then divided into three different classes. In this case, each vegetation class was attributed the same sinuosity value as that of the channel bordering it (Figure 3b).

To perform this operation, the network skeleton was imported into the GIS software, each branch was converted into a polyline with its sinuosity as an attribute, and then a spatial analysis was performed with respect to the vegetation map layer. Based on their spatial location, vegetation polygons were joined to the channel network layer and were given the sinuosity attributes of the channel closest to their boundaries. The nearest channel is defined as the one that is geographically closest to the boundary of the vegetation patch: proximity is based on the Euclidean distance, which is the straight-line distance between the features. The distance in meters between the polygon and the channel was recorded, and polygons with a maximum distance of ~40 m (equal to 2 pixels in the SPOT image) from a channel were included in the statistical analysis on plant distribution and sinuosity.

4. Results

4.1. Image Classification and Validation

The vegetation classification of the SPOT 2012 image (Figure 4) was validated against the RWS vegetation map of the Saeftinghe salt marsh (2010). Our classification identified the *E. athericus* vegetation class with the highest accuracy (95%). The classification of the other two classes (i.e., pioneer vegetation and reed stands) showed lower accuracy, and there was an underestimation of the high vegetation zone, mainly for

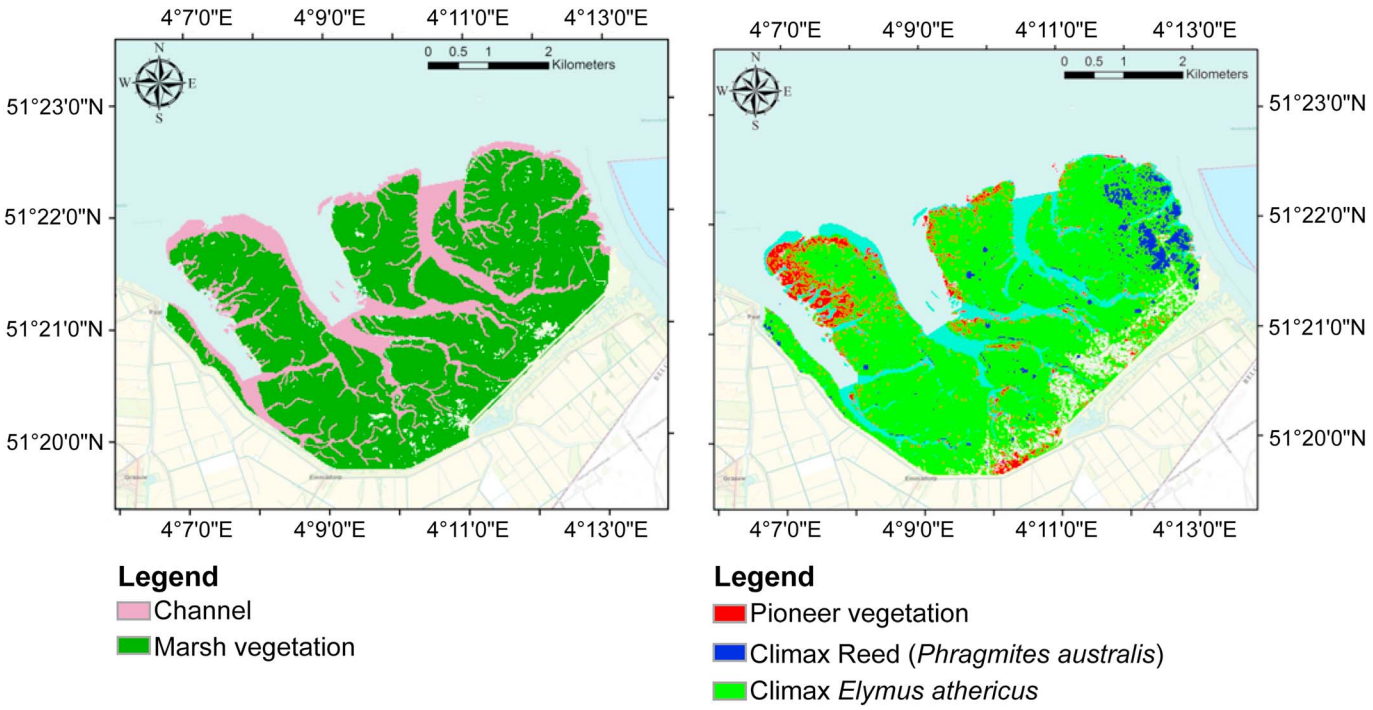

Figure 4. Classification of the SPOT-4 image (July 2012) for the Saeftinghe salt marsh. (left) Classification of channel network and vegetated salt marsh. (right) Classification of the vegetated marsh into three different vegetation classes. SPOT-4 = Satellite Pour l'Observation de la Terre 4.

E. athericus, which is the dominant species in the Saeftinghe area (Table 2). The differences between the LSMA classification and the high-resolution RWS map were due to the validation methodology, which for the LSMA classification was mainly based on field radiometry (Rapinel et al., 2015; Small, 2002).

4.2. Relationship Between Vegetation Type and Patch-Size Distribution

For the SPOT 2012 image, a total of 2,469 patches were mapped. The results of the power law analysis for the three different vegetation classes show that their size-frequency distributions are consistent with power laws (Figure 5), with patches being present over a significant range of scales (KS statistic, $p > 0.1$). Therefore, the distribution shows a signal of self-organization. In the *E. athericus* vegetation class, the observed values deviate from the power law in the upper tail of the distribution. This deviation indicates that there are more large patches than would be expected in the power law tail. Among the three classes, the pioneer vegetation has the highest scaling exponent (Figure 5), highlighting that smaller patches are more abundant in this class.

4.3. Relationship Between Channel Sinuosity and Vegetation Patch Size and Type

To investigate the relationship between patch size and maximum channel sinuosity, and whether the relationship holds true at various spatial scales, we first analyzed the 2010 vegetation map (DTM) and then repeated this analysis on the two SPOT-4 satellite acquisitions (1999 and 2012). The patch sizes calculated for the vegetation map and both SPOT-4 images were related to channel sinuosity for each vegetation typology (Figure 6). The relationship between patch size and maximum channel sinuosity calculated for the vegetation map showed a significant negative logarithmic relationship, where high-sinuosity channels were mainly associated with small patches, and large patches were always associated with low-sinuosity channels. This pattern was independent of vegetation type and was significant for all three vegetation classes ($r^2 = 0.47$, $p < 0.0001$ for pioneer vegetation; $r^2 = 0.48$, $p < 0.0001$ for *Elymus* vegetation; and $r^2 = 0.34$, $p = 0.0004$ for reed vegetation).

When the spatial resolution is decreased (SPOT images), the negative logarithmic relationship between patch size and sinuosity is maintained: in the SPOT 1999 image, the relationship is significant for all three vegetation classes ($r^2 = 0.33$, $p = 0.0004$ for pioneer vegetation; $r^2 = 0.19$, $p = 0.02$ for *Elymus* vegetation; and $r^2 = 0.48$,

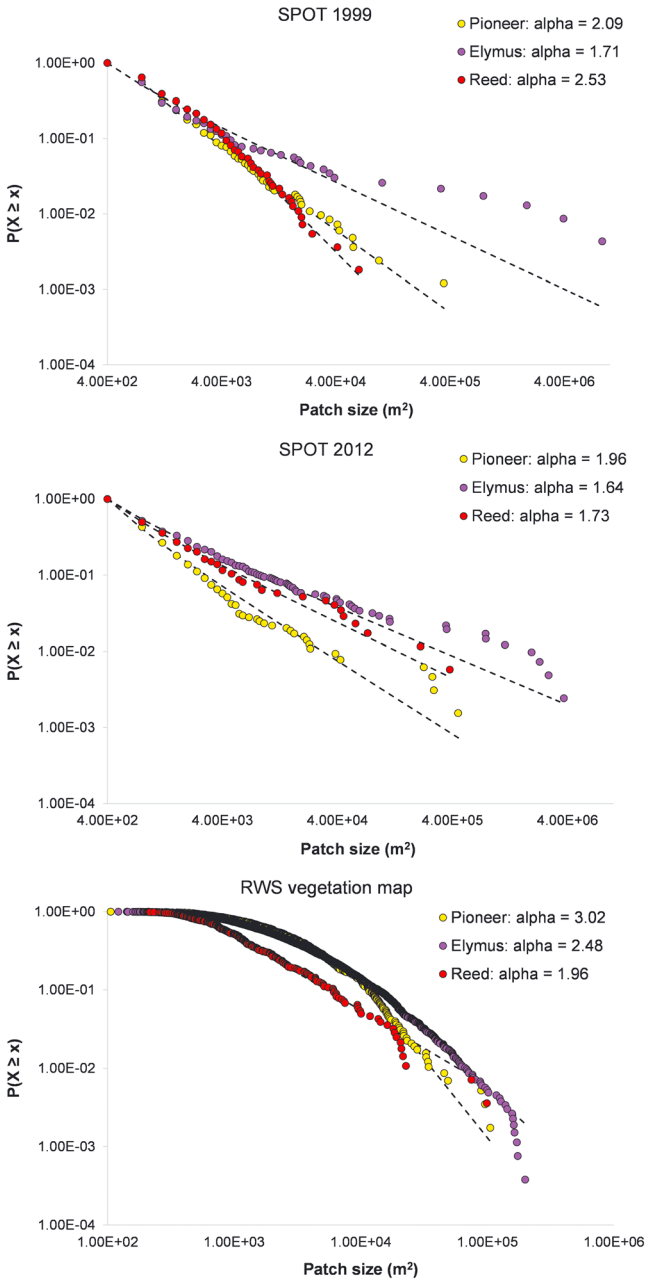

Figure 5. Patch-size distribution of pioneer (yellow), *Elymus athericus* (purple), and reed (*P. australis*) vegetation (red) of the classification of the two SPOT-4 satellite images (1999 and 2012) and the RWS vegetation map (2010) for the Saeftinghe salt marsh. The *x* axis indicates the size of each patch (as number of pixels), and the *y* axis indicates the frequency of each patch size. The graph is in log-log scale, with the dotted line representing the distributional model and the circles representing the observed data. SPOT-4 = Satellite Pour l'Observation de la Terre 4; RWS = Rijkswaterstaat.

$p = 0.0001$ for reed vegetation). In the SPOT 2012 image, the relationship is significant for the pioneer and *Elymus* vegetation ($r^2 = 0.44$, $p = 0.001$ and $r^2 = 0.26$, $p = 0.003$, respectively) but not for the reed vegetation class ($r^2 = 0.21$, $p = 0.09$). In addition, considering the images of 1999, 2010, and 2012, the temporal trend suggests a decrease in the largest patch sizes and an increase in channel sinuosity for both the pioneer and the *Elymus* vegetation but not the reed vegetation.

A comparison of the distribution of the channel sinuosity values among vegetation types for the RWS 2010 map revealed no significant difference in average sinuosity among the three classes (one-way analysis if variance [ANOVA], $F_{2, 3203} = 1.863$, $p = 0.155$; Figure 7a). By repeating the analysis on the SPOT 1999 image, significant differences were found in sinuosity between vegetation types (one-way ANOVA, $F_{2, 1610} = 17.75$, $p < 0.001$; Figure 7b), with significantly higher sinuosity in the reed class than in the pioneer and *Elymus* vegetation (Tukey's Honest Significant Difference [HSD], $p < 0.001$ and $p = 0.01$, respectively); however, no significant difference was found between the pioneer and *Elymus* vegetation (Tukey's HSD, $p = 0.43$). The analysis of the SPOT 2012 image also revealed significant differences in sinuosity among vegetation types (one-way ANOVA, $F_{2, 1102} = 3.982$, $p = 0.01$; Figure 7c), with significantly higher sinuosity in the *Elymus* class than in the pioneer vegetation (Tukey's HSD, $p = 0.03$) but not in the reed class (Tukey's HSD, $p = 0.09$). Within each vegetation type, significant differences in average sinuosity between years were found in both pioneer vegetation and *Elymus* but not in the reed class (Wilcoxon rank sum test, $W = 28775$, $p = 0.36$). In the pioneer vegetation, average sinuosity increased significantly over time from 1999 to 2012 (Wilcoxon rank sum test, $W = 227000$, $p < 0.0001$). In the *Elymus* class, average sinuosity increased significantly from 1999 to 2012 (Wilcoxon rank sum test, $W = 32968$, $p = 0.0002$).

According to Lazarus and Constantine (2013), the value of roughness relative to slope (R/S) controls sinuosity rather than the roughness linked to topography and vegetation density or slope. The illumination reflection is determined by the salt marsh orientation and the location of the Sun. This relationship (between salt marsh orientation, Sun location, and illumination reflection) has been explored previously (Gu & Gillespie, 1998; Riaño & Chuvieco, 2003). Thus, it is assumed that the first-order reflected illumination can be determined from the incidence (illumination) angle. Therefore, we recalculated the substrate and vegetation fractions by partitioning the removed topographic shadow (~50%) among the substrate and vegetation in proportion to their respective contributions to the non-shadow fraction. Thus, the fraction added or removed from the dark end-member was distributed proportionally to the dark and vegetation end-members, allowing us to match a coarse-scale vegetation analysis to a comparably coarse channel network; we assumed that a mostly flat surface should have no change after correction, and the Sun-facing and Sun-backing slopes should have the same removable linear trend (Kane et al., 2008). The results show that when the slope exceeds the resistance term ($R/S < 1$), the pioneer vegetation types exhibit lower sinuosity, while the *Elymus* vegetation types exhibit higher sinuosity (Figure 8).

The equation of the linear dark shadow function that we used incorporates the Sun elevation and azimuth information that represent the specific time of interest, and this includes the slope (including vegetation roughness) and the azimuth information derived from the DTM. The LIDAR DTM data were, in fact, subset

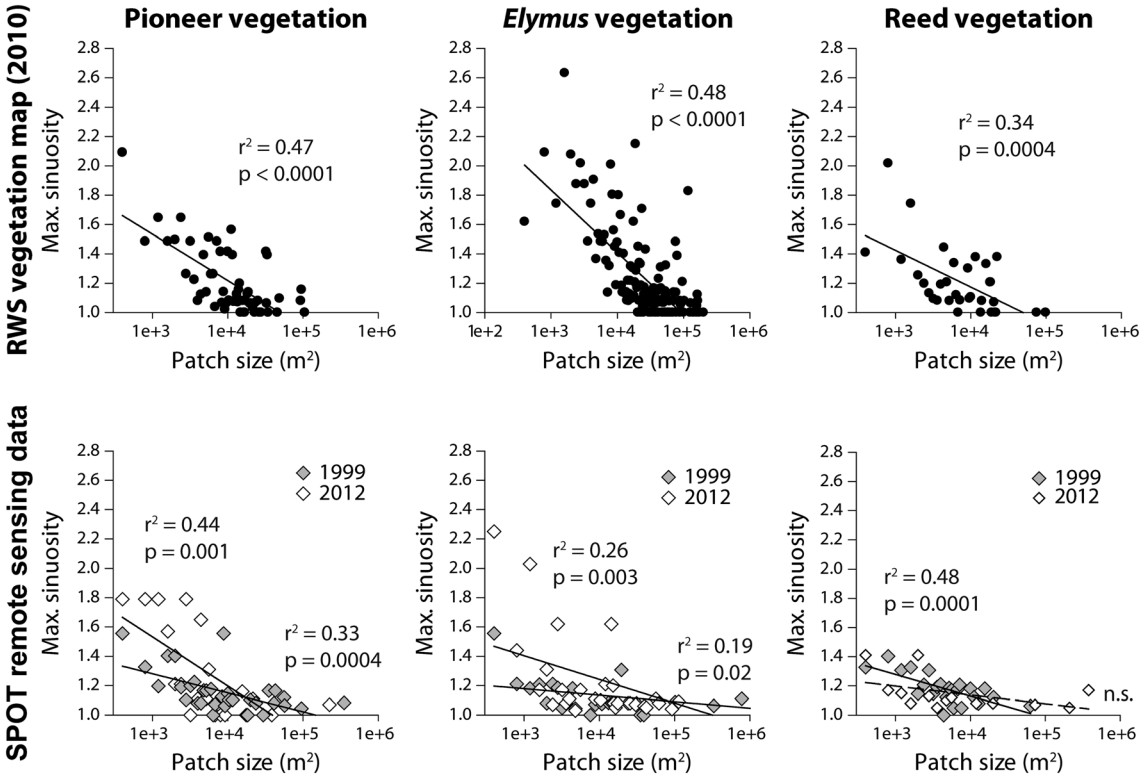

Figure 6. – Relationships between vegetation patch size (m^2, log. Scale) and maximum sinuosity of the adjacent channel, on both the high-resolution RWS vegetation map from 2010 and the two SPOT remote sensing images from 1999 and 2012. The relationships are shown for each of the three main vegetation typologies (e.g., pioneer, *Elymus* and reed vegetation). SPOT = Satellite Pour l'Observation de la Terre; RWS = Rijkswaterstaat.

to be the same size as each SPOT, and the solar incidence angle was calculated. Thus, sinuosity seemed to be higher for *Elymus* than for pioneer vegetation where there was moderate vegetation roughness with very low slope.

4.4. Relationship Among Marsh Elevation, Vegetation Type, and Patch Size

We found no significant relationship between patch size and marsh elevation for the *Elymus* and reed vegetation in the RWS map (r^2 = 0.0001, p = 0.51 and r^2 = 0.009, p = 0.11; Figure 9a). The relationship was

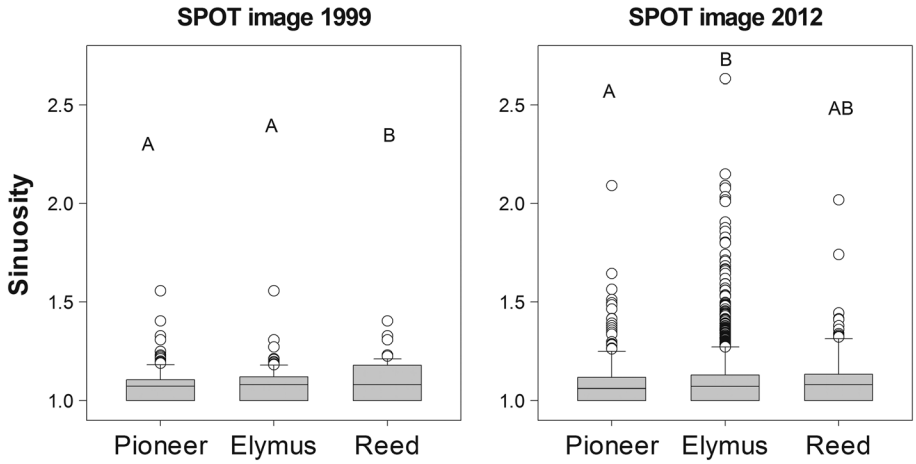

Figure 7. Boxplot of the distribution of channel sinuosity values within each vegetation typology, on the RWS vegetation map and on the SPOT satellite images from 1999 and 2012. Different letters denote significant differences among the three vegetation classes (ANOVA, p = 0.05). SPOT = Satellite Pour l'Observation de la Terre; RWS = Rijkswaterstaat; ANOVA = analysis of variance.

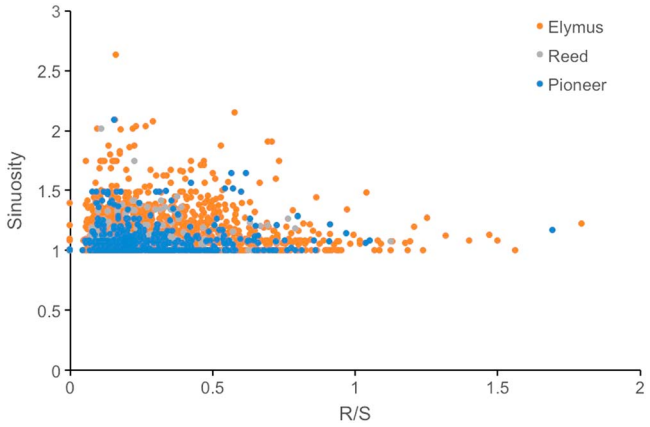

Figure 8. Plot of sinuosity versus *R/S* values using the equation of the linear dark shadow function. The trend does not contradict that of Lazarus & Constantine (2013); we have much higher *R/S* values due to the scale factor of the two SPOT image resolutions to which we have resampled the DTM. SPOT = Satellite Pour l'Observation de la Terre; DTM = digital terrain model.

significant for pioneer vegetation, and patch size slightly increased with elevation; however, this relationship had a low regression coefficient that explained only 7% of the variance ($r^2 = 0.07$, $p = 0.04$).

The relationship between vegetation type and elevation showed that each of the three vegetation classes was located within different soil elevation ranges in the marsh, with pioneer vegetation occupying the lowest areas of the marsh, *Elymus* vegetation occupying the intermediate zone, and reed occupying the highest elevation zones (Figure 9b). The elevation ranges are relatively narrow, with standard deviations of 4.4, 3.1, and 3.8 cm for the three vegetation types, respectively.

5. Discussion

In the present study, we performed an analysis of the relationship between vegetation patterns (i.e., vegetation type and patchiness) and salt marsh geomorphology (viz. channel geometry, i.e., sinuosity and elevation) of three RS-based data sets of a Dutch salt marsh obtained in three different years and with different spatial resolutions (2–20 m).

Our results first show that the patch-size distributions of the three main vegetation types (pioneer, *Elymus* and reed) are consistent with power law relationships (Figure 5), implying there was scale invariance and a lack of characteristic patch size. This result indicates the presence of self-organizational processes that are mediated by scale-dependent biogeomorphic feedback mechanisms (Pascual et al., 2002; Rietkerk & van de Koppel, 2008; Weerman et al., 2010, 2012). These observations support recent hypotheses on the importance of reciprocal interaction feedbacks between vegetation establishment and channel formation in salt marshes (Bouma et al., 2007, 2009; Temmerman et al., 2007). To our knowledge, however, such feedbacks have only been reported for pioneer vegetation thus far. The fact that similar power law relations are observed in vegetation types typical of later successional stages in salt marshes either implies that similar biogeomorphical feedback mechanisms are actually at play in more mature salt marsh vegetation as well or this result could imply that these patterns are *inherited* from the pioneer stage as *Elymus* and reed become established.

Second, we observed an inverse logarithmic relationship between patch size and channel sinuosity, which was independent of vegetation type and also independent of differences in plant structure and abundance (fractional cover) between these vegetation types as well as the elevational ranges within which they occur. Small vegetation patches are consistently found along channels with higher sinuosity ($s > 1.5$), while larger patches are associated with almost straight-line paths ($s \approx 1$; Figure 6). These findings corroborate studies that show that the establishment of vegetation on bare tidal flats (but also in fluvial systems) (Gabet et al., 2014; Tal & Paola, 2010) leads to a marked change in channel geometry (Millar, 2000), with increases in channel

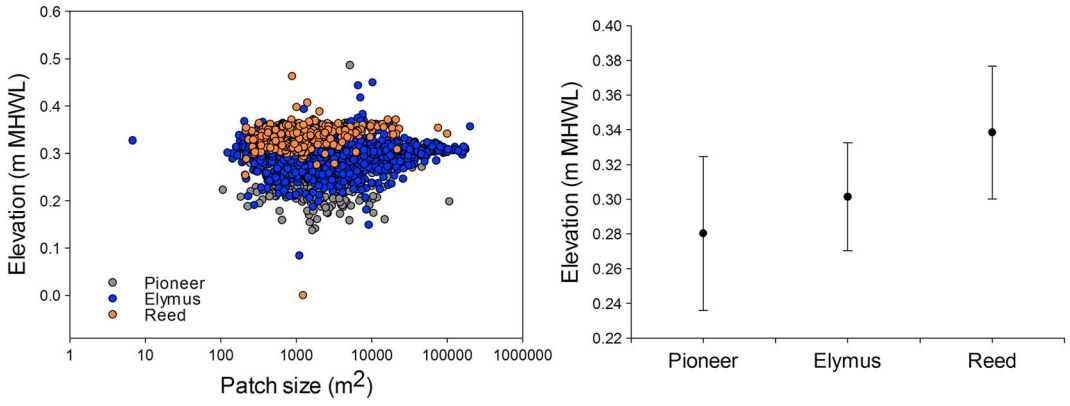

Figure 9. (left) Relationship between patch size (m^2) and marsh elevation (m) by vegetation typology. (right) Soil elevation ranges for the pioneer, *Elymus*, and reed vegetation in the marsh (mean ± SD). SD = standard deviation.

drainage density and channel network efficiency (Kearney & Fagherazzi, 2016; Temmerman et al., 2007; Vandenbruwaene et al., 2012). These changes are most likely related to increases in channel branching and/or meandering. Our analyses confirm that initial vegetation colonization in the form of small patches will result in high sinuosity values, considering that the feedback between vegetation and sedimentation allows the *pioneer* part of the marsh to gain elevation where incipient salt-marsh deposition starts developing (D'Alpaos et al., 2017). Moreover, our findings are in agreement with model predictions of sinuosity (D'Alpaos et al., 2007; Marani et al., 2010, 2002; Lazarus & Constantine, 2013; Schwarz et al., 2014), with increasing vegetation fractional cover and, hence, increasing flow resistance.

Based on the above observations, we propose the following scenario for the evolution of sinuosity during salt marsh development.

1. The settlement of minimum pioneer vegetation patches (e.g., *Spartina* spp.) on bare tidal flats enhance channel formation (maximum sinuosity) but also increase drainage density and channel efficiency (e.g., Kearney & Fagherazzi, 2016; Temmerman et al., 2007; Vandenbruwaene et al., 2012). These characteristics are limited at the pioneer stage and confirmed by the *R*/*S* relationship, which shows that the resistance term is not strong enough relative to the slope to force higher sinuosity (Figure 8). The drainage network that develops during the pioneer stage establishes the template for vegetation succession.
2. Up on the marsh platform, we observe that where slope is low, the effect of the roughness term is greatest, as *Elymus* takes over (the largest and smallest patches are all in the *Elymus*, Figures 5 and 6), suggesting that the interaction between sinuosity and patch size with channel density is positively related to vegetation abundance (fractional cover, Temmerman et al., 2007). Where the channel network is relatively weak (i.e., experiences less frequent flushing), patch merging might overprint channels to create large patches (D'Alpaos, Lanzoni, Marani, Fagherazzi, Rinaldo, 2005; D'Alpaos et al., 2007; Thomson et al., 2004). This process occurs where models predict that the merging of small pioneer patches into larger patches leads to enhanced channel erosion and, finally, to the emergence of a salt marsh platform that is dissected by tidal channels (Kirwan & Murray, 2008a, 2008b; D'Alpaos et al., 2010; Hu et al., 2015).
3. The fact that the observed power law patch-size distributions and the patch size-sinuosity relationships are independent of vegetation type (and hence, also vegetation structure, fractional cover, and elevation range) suggests that similar biogeomorphic processes operate under the weak relationship between the sinuosity and slope/roughness effect due to the fractional vegetation cover. This is the case for the reedy portion of the marsh.
4. Late successional vegetation types colonize pioneer patches of different sizes, provided that the ecological conditions are suitable and that further vegetation development will continue to stabilize the preexisting patterns. Interestingly, Vandenbruwaene et al. (2012), in an analysis of long-term change in the same Saeftinghe salt marsh, also observed a lack of further change in channel drainage density (and channel width) once vegetation was established. Of course, this does not mean that no change takes place at all, as further patch mergers can occur in more mature vegetation types (resulting in the largest patch sizes in these vegetation areas, Figure 5); this result confirms an *inheritance* of pioneer stage morphology that then gets amended the most on the flattest parts of the platform (i.e., the smallest and largest patches) where the vegetation effects are dominant.

The LSMA method we propose enables an improved long-term assessment of salt marsh evolution, and it can give rise to a new methodology for detecting vegetation patchiness that could reflect the biotic processes that shape the landscape. The method represents a significant step forward in respect to using classical NDVI for vegetation detection (Kearney & Fagherazzi, 2016), and this step is necessary when considering the complexity of ecological processes, such as vegetation succession, particularly in highly dynamic ecosystems such as estuaries (Boerema et al., 2016; Bouma et al., 2016). By comparing the patterns in different vegetation types, our methodology provides a tool that can be used to gain information about the interaction of various successional stages of vegetation with geomorphology; this tool can also be used to describe the tidal channel networks as a distinct topographic signature of life (Dietrich & Perron, 2006).

6. Conclusions

Our study aims to enhance process understanding of marsh dynamics by identifying the relation between vegetation and geomorphology using an RS method that has already been tested in other estuaries and

deltas. The methodology we developed and the relations we show among sinuosity, vegetation, patchiness, and elevation at different spatial scales have the potential to provide information on the biogeomorphological evolution of salt marshes over longer timescales using temporal series analysis. In particular, the method enables the study of the relationship between sinuosity and vegetation patch size, irrespective of vegetation type, as the tidal network changes from pioneer to later successional stages. We provide evidence for the degree to which vegetation is related to tidal channel network characteristics in terms of the spatial relationship between vegetation patch size and maximum sinuosity. This reciprocal interaction may modify fundamental processes, such as the fluxes of water and sediment in the marsh, that lead to an increased elevation of the vegetation patches. The intriguing results suggest that vegetation patches in intertidal areas might be interpreted as a topographic signature of life.

Acknowledgments
The final results and the dissemination of the present research is under the Coastal Mapping EU service contract number - EASME/EMFF/2014/1.3.1.4/SI2.708188. The scientific achievement comes from the EU FP7.2009-1, Contract 244104 - THESEUS *Innovative technologies for safer European coasts in a changing climate*. The support of European Space Agency through the Project Cat-1 7963 is gratefully acknowledged. K. S. acknowledges financial support from Ghent University (BOF-GOA 01G01911). We would also like to acknowledge the Flanders Marine Institute (VLIZ), Jeroen Van Wichelen, Renaat Dasseville, and Lander Blommaert for field assistance and logistic support. The ASD Field Spectroradiometer was provided by VITO (Vlaamse Instelling voor Technologisch Onderzoek; Flemish Institute for Technological Research). Data (Spot Images in the different Level 1A, 2A, 2B, 3, Image-based vegetation and sinuosity classification, Field Radiometry, and excel file for data analysis including patch size and synuosity calculation) are available at the ftp://ftp.isprambiente.it/cra/loreta user name mermaid.partner, password: F15FKrtt. The final data set that is also available under the Flanders Marine Institute (VLIZ) shares IMIS information system with a Digital Object Identifier https://doi.org/10.14284/322.

References

Adam, P. (1990). Saltmarsh ecology. In *Cambridge studies in ecology* (125 pp.). Cambridge: Cambridge University Press. https://doi.org/10.1017/CBO9780511565328

Adams, J. B., Smith, M. O., & Johnson, P. E. (1986). Spectral mixture modeling: A new analysis of rock and soil types at the Viking Lander 1 site. *Journal of Geophysical Research*, *91*(B8), 8098–8112. https://doi.org/10.1029/JB091iB08p08098

Allen, J. (2000). Morphodynamics of Holocene salt marshes: A review sketch from the Atlantic and southern North Sea coasts of Europe. *Quaternary Science Reviews*, *19*(12), 1155–1231.

Baeyens, W., van Eck, B., Lambert, C., Wollast, R., & Goeyens, L. (1997). General description of the Scheldt estuary. *Hydrobiologia*, *366*(1/3), 1–14. https://doi.org/10.1023/A:1003164009031

Barbour, J. R. (2008). The origin and significance of sinuosity along incising bedrock rivers, (PhD dissertation, 187 pp.). Columbia University, New York. Last access 18 August 2016, Retrieved from http://www.ldeo.columbia.edu/~jbarbour/thesis/jrb_phd_dissertation.pdf

Beeftink, W. G. (1966). Vegetation and habitat of the salt marshes and beach plains in the south-western part of the Netherlands. *Wentia*, *15*, 83–108. https://doi.org/10.1111/j.1438-8677.1966.tb00021.x

Boardman, J. W. (1993). *Automating spectral unmixing of AVIRIS data using convex geometry concepts*. Paper presented at Summaries 4th Annu. JPL Airborne Geoscience Workshop, JPL Publication 93–26.

Boerema, A., Geerts, L., Oosterlee, L., Temmerman, S., & Meire, P. (2016). Ecosystem service delivery in restoration projects: The effect of ecological succession on the benefits of tidal marsh restoration. *Ecology and Society*, *21*(2), 10.

Boon, J. D. III (1975). Tidal discharge asymmetry in a salt marsh drainage system. *Limnology and Oceanography*, *20*(1), 71–80. https://doi.org/10.4319/lo.1975.20.1.0071

Boon, J. D., & Byrne, R. J. (1981). On basin hypsometry and the morphodynamic response of coastal inlet systems. *Marine Geology*, *40*(1-2), 27–48. https://doi.org/10.1016/0025-3227(81)90041-4

Bouma, T., Friedrichs, M., Van Wesenbeeck, B., Temmerman, S., Graf, G., & Herman, P. (2009). Density-dependent linkage of scale-dependent feedbacks: A flume study on the intertidal macrophyte *Spartina anglica*. *Oikos*, *118*(2), 260–268. https://doi.org/10.1111/j.1600-0706.2008.16892.x

Bouma, T. J., van Belzen, J., Balke, T., van Dalen, J., Klaassen, P., Hartog, A. M., et al. (2016). Short-term mudflat dynamics drive long-term cyclic salt marsh dynamics. *Limnology and Oceanography: Methods*, *61*(6), 2261–2200, 2275. https://doi.org/10.1002/lno.10374

Bouma, T. J., Van Duren, L., Temmerman, S., Claverie, T., Blanco-Garcia, A., Ysebaert, T., & Herman, P. M. J. (2007). Spatial flow and sedimentation patterns within patches of epibenthic structures: Combining field, flume and modelling experiments. *Continental Shelf Research*, *27*(8), 1020–1045. https://doi.org/10.1016/j.csr.2005.12.019

Chander, G., & Markham, B. (2003). Revised Landsat-5 TM radiometric calibration procedures and postcalibration dynamic ranges. *IEEE Transactions on Geoscience and Remote Sensing*, *41*(11), 2674–2677. https://doi.org/10.1109/TGRS.2003.818464

Clauset, A., Shalizi, C. R., & Newman, M. E. (2009). Power-law distributions in empirical data. *SIAM Review*, *51*(4), 661–703. https://doi.org/10.1137/070710111

Corenblit, D., Baas, A., Balke, T., Bouma, T., Fromard, F., Garófano-Gómez, V., et al. (2015). Engineer pioneer plants respond to and affect geomorphic constraints similarly along water–terrestrial interfaces world-wide. *Global Ecology and Biogeography*, *24*(12), 1363–1376. https://doi.org/10.1111/geb.12373

D'Alpaos, A., Ghinassi, M., Finotello, A., Brivio, L., Bellucci, L. G., & Marani, M. (2017). Tidal meander migration and dynamics: A case study from the Venice lagoon. *Marine and Petroleum Geology*, *87*, 80–90. https://doi.org/10.1016/j.marpetgeo.2017.04.012

D'Alpaos, A., Lanzoni, S., Marani, M., Bonometto, A., Cecconi, G., & Rinaldo, A. (2005). Spontaneous tidal network formation within a constructed salt marsh: Observations and morphodynamic modelling. *Geomorphology*, *91*(3-4), 186–197. https://doi.org/10.1016/j.geomorph.2007.04.013

D'Alpaos, A., Lanzoni, S., Marani, M., Fagherazzi, S., & Rinaldo, A. (2005). Tidal network ontogeny: Channel initiation and early development. *Journal of Geophysical Research*, *110*, F02001. https://doi.org/10.1029/2004JF000182

D'Alpaos, A., Lanzoni, S., Marani, M., & Rinaldo, A. (2007). Landscape evolution in tidal embayments: Modeling the interplay of erosion, sedimentation, and vegetation dynamics. *Journal of Geophysical Research*, *112*, F01008. https://doi.org/10.1029/2006JF000537

D'Alpaos, A., Lanzoni, S., Marani, M., & Rinaldo, A. (2010). On the tidal prism—Channel area relations. *Journal of Geophysical Research*, *115*, F01003. https://doi.org/10.1029/2008JF001243

D'Alpaos, A., Lanzoni, S., Mudd, S. M., & Fagherazzi, S. (2006). Modeling the influence of hydroperiod and vegetation on the cross-sectional formation of tidal channels. *Estuarine, Coastal and Shelf Science*, *69*(3-4), 311–324. https://doi.org/10.1016/j.ecss.2006.05.002

Defina, A., Carniello, L., Fagherazzi, S., & D'Alpaos, L. (2007). Self-organization of shallow basins in tidal flats and salt marshes. *Journal of Geophysical Research*, *112*, F03001. https://doi.org/10.1029/2006JF000550

Dietrich, W. E., & Perron, J. T. (2006). The search for a topographic signature of life. *Nature*, *439*(7075), 411–418. https://doi.org/10.1038/nature04452

Fagherazzi, S. (2008). Self-organization of tidal deltas. *Proceedings of the National Academy of Sciences of the United States of America*, *105*(48), 18,692–18,695. https://doi.org/10.1073/pnas.0806668105

Fagherazzi, S., Bortoluzzi, A., Dietrich, W. E., Adami, A., Lanzoni, S., Marani, M., & Rinaldo, A. (1999). Tidal networks: 1. Automatic network extraction and preliminary scaling features from digital terrain maps. *Water Resources Research*, *35*(12), 3891–3904. https://doi.org/10.1029/1999WR900236

Fagherazzi, S., Carniello, L., D'Alpaos, L., & Defina, A. (2006). Critical bifurcation of shallow microtidal landforms in tidal flats and salt marshes. *Proceedings of the National Academy of Sciences of the United States of America*, *103*(22), 8337–8341. https://doi.org/10.1073/pnas.0508379103

Fagherazzi, S., & Furbish, D. J. (2001). On the shape and widening of salt marsh creeks. *Journal of Geophysical Research*, *106*, 991–1003.

Fagherazzi, S., Hannion, M., & D'Odorico, P. (2008). Geomorphic structure of tidal hydrodynamics in salt marsh creeks. *Water Resources Research*, *44*, W02419. https://doi.org/10.1029/2007WR006289

Fagherazzi, S., Kirwan, M. L., Mudd, S. M., Guntenspergen, G. R., Temmerman, S., D'Alpaos, A., et al. (2012). Numerical models of salt marsh evolution: Ecological, geomorphic, and climatic factors. *Reviews of Geophysics*, *50*, RG1002. https://doi.org/10.1029/2011RG000359

Fagherazzi, S., Marani, M., & Blum, L. K. (2004). Introduction: The coupled evolution of geomorphological and ecosystem structures in salt marshes. In S. Fagherazzi, M. Marani, & L. K. Blum (Eds.), *The ecogeomorphology of tidal marshes, coastal estuarine study* (Vol. 59, pp. 1–5). Washington, DC: American Geophysical Union. https://doi.org/10.1029/CE059

Fagherazzi, S., & Sun, T. (2004). A stochastic model for the formation of channel networks in tidal marshes. *Geophysical Research Letters*, *31*, L21503. https://doi.org/10.1029/2004GL020965

Filipponi, F., Valentini, E., Nguyen Xuan, A., Guerra, C., Andrzejak, F. W. M., & Taramelli, A. (2018). Global MODIS fraction of green vegetation cover for monitoring vegetation abrupt and gradual changes. *Remote Sensing*, *10*(4), 653. https://doi.org/10.3390/rs10040653

Forster, R. M., & Jesus, B. (2006). Field spectroscopy of estuarine intertidal habitats. *International Journal of Remote Sensing*, *27*, 3657–3669.

Foti, R., & Ramírez, J. (2013). A mechanistic description of the formation and evolution of vegetation patterns. *Hydrology and Earth System Sciences*, *17*(1), 63–84. https://doi.org/10.5194/hess-17-63-2013

Frazier, P. S., & Page, K. G. (2000). Water body detection and delineation with Landsat TM data. *Photogrammetric Engineering & Remote Sensing*, *66*(12), 1461–1467.

French, J. (2006). Tidal marsh sedimentation and resilience to environmental change: Exploratory modeling of tidal, sea-level, and sediment supply forcing in predominantly allochthonous systems. *Marine Geology*, *235*(1-4), 119–136. https://doi.org/10.1016/j.margeo.2006.10.009

French, J. R. (1993). Numerical simulation of vertical marsh growth and adjustment to accelerated sea-level rise, North Norfolk, UK. *Earth Surface Processes and Landforms*, *18*(1), 63–81. https://doi.org/10.1002/esp.3290180105

French, J. R., & Stoddart, D. R. (1992). Hydrodynamics of salt marsh creek systems: Implications for marsh morphological development and material exchange. *Earth Surface Processes and Landforms*, *17*(3), 235–252. https://doi.org/10.1002/esp.3290170304

Friedrichs, C. T. (1995). Stability shear stress and equilibrium cross-sectional geometry of sheltered tidal channels. *Journal of Coastal Research*, *11*(4), 1062–1074.

Friedrichs, C. T., & Aubrey, D. G. (1988). Non-linear tidal distortion in shallow well-mixed estuaries: A synthesis. *Estuarine, Coastal and Shelf Science*, *27*(5), 521–545. https://doi.org/10.1016/0272-7714(88)90082-0

Gabet, E. J., Perron, J. T., & Johnson, D. L. (2014). Biotic origin for Mima mounds supported by numerical modeling. *Geomorphology*, *206*, 58–66. https://doi.org/10.1016/j.geomorph.2013.09.018

Garofalo, D. (1980). The influence of wetland vegetation on tidal stream channel migration and morphology. *Estuaries*, *3*(4), 258–270. https://doi.org/10.2307/1352081

Gonzalez, R. C., Woods, R. E., & Eddins, S. R. (2004). *Digital image processing using MATLAB*. New Jersey: Pearson Prentice Hall.

Gu, D., & Gillespie, A. (1998). Topographic normalization of Landsat TM images of forest based on subpixel sun-canopy-sensor geometry. *Remote Sensing of Environment*, *64*, 166–175.

Hladik, C., Schalles, J., & Alber, M. (2013). Salt marsh elevation and habitat mapping using hyperspectral and LIDAR data. *Remote Sensing of Environment*, *139*, 318–330. https://doi.org/10.1016/j.rse.2013.08.003

Hu, Z., Belzen, J., Wal, D., Balke, T., Wang, Z. B., Stive, M., & Bouma, T. J. (2015). Windows of opportunity for salt marsh vegetation establishment on bare tidal flats: The importance of temporal and spatial variability in hydrodynamic forcing. *Journal of Geophysical Research: Biogeosciences*, *120*, 1450–1469. https://doi.org/10.1002/2014JG002870

Ibrahim, E., & Monbaliu, J. (2011). Suitability of spaceborne multispectral data for inter-tidal sediment characterization: A case study. *Estuarine, Coastal and Shelf Science*, *92*, 437–445.

Janssen, J. A. M. (2001). Monitoring of salt-marsh vegetation by sequential mapping, (PhD dissertation, 249 pp.). University of Amsterdam, Amsterdam, The Netherlands.

Jefferies, R. L., Jano, A. P., & Abraham, K. F. (2006). A biotic agent promotes large-scale catastrophic change in the coastal marshes of Hudson Bay. *Journal of Ecology*, *94*(1), 234–242. https://doi.org/10.1111/j.1365-2745.2005.01086.x

Johnson, P. E., Smith, M. O., Taylor-George, S., & Adams, J. B. (1983). A semiempirical method for analysis of the reflectance spectra of binary mineral mixtures. *Journal of Geophysical Research*, *88*(B4), 3557–3561. https://doi.org/10.1029/JB088iB04p03557

Kane, V., Gillespie, A., & McGaughey, R. (2008). Interpretation and topographic compensation of conifer canopy self-shadowing. *Remote Sensing of Environment*, *112*(10), 3820–3832. https://doi.org/10.1016/j.rse.2008.06.001

Kearney, W. S., & Fagherazzi, S. (2016). Salt marsh vegetation promotes efficient tidal channel networks. *Nature Communications*, *7*. https://doi.org/10.1038/ncomms12287

Kirwan, M. L., & Murray, A. B. (2008a). Tidal marshes as disequilibrium landscapes? Lags between morphology and Holocene sea level change. *Geophysical Research Letters*, *35*, L24401. https://doi.org/10.1029/2008GL036050

Kirwan, M. L., & Murray, A. B. (2008b). Ecological and morpho-logical response of brackish tidal marshland to the next century of sea level rise: Westham Island, British Columbia. *Global and Planetary Change*, *60*(3-4), 471–486. https://doi.org/10.1016/j.gloplacha.2007.05.005

Kirwan, M. L., Temmerman, S., Skeehan, E. E., Guntenspergen, G. R., & Fagherazzi, S. (2016). Overestimation of marsh vulnerability to sea level rise. *Nature Climate Change*, *6*(3), 253–260. https://doi.org/10.1038/nclimate2909

Lazarus, E. D., & Constantine, J. A. (2013). Generic theory for channel sinuosity. *Proceedings of the National Academy of Sciences*, *110*(21), 8447–8452. https://doi.org/10.1073/pnas.1214074110

Manzo, C., Valentini, E., Taramelli, A., Filipponi, F., & Disperati, L. (2014). Spectral characterization of coastal sediments using field spectral libraries, airborne hyperspectral images and topographic lidar data (FHyL). *International Journal of Applied Earth Observation and Geoinformation*, *36*, 54–68. https://doi.org/10.1016/j.jag.2014.11.003

Marani, M., Belluco, E., Ferrari, S., Silvestri, S., D'Alpaos, A., Lanzoni, S., et al. (2006). Analysis, synthesis and modelling of high-resolution observations of salt marsh eco-geomorphological patterns in the Venice lagoon. *Estuarine, Coastal and Shelf Science*, *69*(3–4), 414–426. https://doi.org/10.1016/j.ecss.2006.05.021

Marani, M., D'Alpaos, A., Lanzoni, S., Carniello, L., & Rinaldo, A. (2010). The importance of being coupled: Stable states and catastrophic shifts in tidal biomorphodynamics. *Journal of Geophysical Research*, *115*, F04004. https://doi.org/10.1029/2009JF001600

Marani, M., Lanzoni, S., Belluco, E., D'Alpaos, A., Defina, A., & Rinaldo, A. (2003). On the drainage density of tidal networks. *Water Resources Research*, *39*(2), 1040. https://doi.org/10.1029/2001WR001051

Marani, M., Lanzoni, S., Zandolin, D., Seminara, G., & Rinaldo, A. (2002). Tidal meanders. *Water Resources Research*, *38*(11), 1225. https://doi.org/10.1029/2001WR000404

Maréchal, C., Pottier, E., Hubert-Moy, L., & Rapinel, S. (2012). One year wetland survey investigations from quad-pol RADARSAT-2 time-series SAR images. *Canadian Journal of Remote Sensing*, *38*(3), 240–252. https://doi.org/10.5589/m12-017

Mariotti, G., & Fagherazzi, S. (2010). A numerical model for the coupled long-term evolution of salt marshes and tidal flats. *Journal of Geophysical Research*, *115*, F01004. https://doi.org/10.1029/2009JF001326

Mason, D. C., Scott, T. R., & Wang, H. J. (2006). Extraction of tidal channel networks from airborne scanning laser altimetry. *ISPRS Journal of Photogrammetry and Remote Sensing*, *61*(2), 67–83. https://doi.org/10.1016/j.isprsjprs.2006.08.003

Meire, P., Ysebaert, T., Van Damme, S., Van den Bergh, E., Maris, T., & Struyf, E. (2005). The Scheldt estuary: A description of a changing ecosystem. *Hydrobiologia*, *540*(1–3), 1–11. https://doi.org/10.1007/s10750-005-0896-8

Méléder, V., Launeau, P., Barillé, L., Combe, J.-P., Carrère, V., Jesus, B., & Verpoorter, C. (2010). Hyperspectral imaging for mapping microphytobenthos in coastal areas. In M. Maanan & M. Robin (Eds.), *Geomatic solutions for coastal environment* (pp. 71–139). Hauppague, New York: Nova Science Publishers, Inc.

Millar, R. G. (2000). Influence of bank vegetation on alluvial channel patterns. *Water Resources Research*, *36*(4), 1109–1118. https://doi.org/10.1029/1999WR900346

Moffett, K. B., Nardin, W., Silvestri, S., Wang, C., & Temmerman, S. (2015). Multiple stable states and catastrophic shifts in coastal wetlands: Progress, challenges, and opportunities in validating theory using remote sensing and other methods. *Remote Sensing*, *7*(8), 10,184–10,226. https://doi.org/10.3390/rs70810184

von Neumann, J. (1951). Various techniques used in connection with random digits. *National Bureau of Standards Applied Math Series*, *12*, 36–38.

Newman, M. E. (2005). Power laws, Pareto distributions and Zipf's law. *Contemporary Physics*, *46*(5), 323–351. https://doi.org/10.1080/00107510500052444

Novakowski, K. I., Torres, R., Gardner, L. R., & Voulgaris, G. (2004). Geomorphic analysis of tidal creek networks. *Water Resources Research*, *40*, W05401. https://doi.org/10.1029/2003WR002722

Pascual, M., Roy, M., Guichard, F., & Flierl, G. (2002). Cluster size distributions: Signatures of self-organization in spatial ecologies. *Philosophical Transactions of the Royal Society B*, *357*(1421), 657–666. https://doi.org/10.1098/rstb.2001.0983

Passalacqua, P., Lanzoni, S., Paola, C., & Rinaldo, A. (2013). Geomorphic signatures of deltaic processes and vegetation: The Ganges-Brahmaputra-Jamuna case study. *Journal of Geophysical Research: Earth Surface*, *118*, 1838–1849. https://doi.org/10.1002/jgrf.20128

Perron, J. T., & Fagherazzi, S. (2012). The legacy of initial conditions in landscape evolution. *Earth Surface Processes and Landforms*, *37*(1), 52–63. https://doi.org/10.1002/esp.2205

Pestrong, R. (1965). The development of drainage patterns on tidal marshes, Stanford Publ. Geol. Sci. Tech. Rep. 10 (87 pp.). Stanford University Stanford, CA.

Pethick, J. S. (1980). Velocity surges and asymmetry in tidal channels. *Estuarine and Coastal Marine Science*, *11*(3), 331–345. https://doi.org/10.1016/S0302-3524(80)80087-9

Rapinel, S., Bouzillé, J. B., Oszwald, J., & Bonis, A. (2015). Use of bi-seasonal Landsat-8 imagery for mapping marshland plant community combinations at the regional scale. *Wetlands*, *35*(6), 1043–1054. https://doi.org/10.1007/s13157-015-0693-8

Riaño, D., & Chuvieco, F. (2003). Assessment of different topographic corrections in Landsat-TM data for mapping vegetation types. *IEEE Transactions on Geoscience and Remote Sensing*, *41*(5), 1056–1061. https://doi.org/10.1109/TGRS.2003.811693

Rietkerk, M., & van de Koppel, J. (2008). Regular pattern formation in real ecosystems. *Trends in Ecology & Evolution*, *23*(3), 169–175. https://doi.org/10.1016/j.tree.2007.10.013

Rinaldo, A., Fagherazzi, S., Lanzoni, S., Marani, M., & Dietrich, W. E. (1999a). Tidal networks: 2. Watershed delineation and comparative network morphology. *Water Resources Research*, *35*(12), 3905–3917. https://doi.org/10.1029/1999WR900237

Rinaldo, A., Fagherazzi, S., Lanzoni, S., Marani, M., & Dietrich, W. E. (1999b). Tidal networks: 3. Landscape-forming discharges and studies in empirical geomorphic relationships. *Water Resources Research*, *35*(12), 3919–3929. https://doi.org/10.1029/1999WR900238

Scanlon, T. M., Caylor, K. K., Levin, S. A., & Rodriguez-Iturbe, I. (2007). Positive feedbacks promote power-law clustering of Kalahari vegetation. *Nature*, *449*(7159), 209–212. https://doi.org/10.1038/nature06060

Schoelynck, J., De Groote, T., Bal, K., Vandenbruwaene, W., Meire, P., & Temmerman, S. (2012). Self-organised patchiness and scale-dependent bio-geomorphic feedbacks in aquatic river vegetation. *Ecography*, *35*(8), 760–768. https://doi.org/10.1111/j.1600-0587.2011.07177.x

Schwarz, C., Bouma, T. J., Zhang, L. Q., Temmerman, S., Ysebaert, T., & Herman, P. M. J. (2015). Interactions between plant traits and sediment characteristics influencing species establishment and scale-dependent feedbacks in salt marsh ecosystems. *Geomorphology*, *250*, 298–307. https://doi.org/10.1016/j.geomorph.2015.09.013

Schwarz, C., Ye, Q. H., Wal, D., Zhang, L. Q., Bouma, T., Ysebaert, T., & Herman, P. M. J. (2014). Impacts of salt marsh plants on tidal channel initiation and inheritance. *Journal of Geophysical Research: Earth Surface*, *119*, 385–400. https://doi.org/10.1002/2013JF002900

Silvestri, S., Marani, M., & Marani, A. (2003). Hyperspectral remote sensing of salt marsh vegetation, morphology and soil topography. *Physics and Chemistry of the Earth, Parts A/B/C*, *28*(1-3), 15–25. https://doi.org/10.1016/S1474-7065(03)00004-4

Silvestri, S., Marani, M., Settle, J., Benvenuto, F., & Marani, A. (2002). Salt marsh vegetation radiometry—Data analysis and scaling. *Remote Sensing of Environment*, *80*(3), 473–482. https://doi.org/10.1016/S0034-4257(01)00325-X

Small, C. (2002). Multitemporal analysis of urban reflectance. *Remote Sensing of Environment*, *81*(2-3), 427–442. https://doi.org/10.1016/S0034-4257(02)00019-6

Small, C. (2004). The Landsat ETM+ spectral mixing space. *Remote Sensing of Environment*, *93*(1), 1–17.

Small, C., & Milesi, C. (2013). Multi-scale standardized spectral mixture models. *Remote Sensing of Environment*, *136*, 442–454. https://doi.org/10.1016/j.rse.2013.05.024

Small, C., & Sohn, R. (2015). Correlation scales of digital elevation models in developed coastal environments. *Remote Sensing of Environment*, *159*, 80–85. https://doi.org/10.1016/j.rse.2014.11.031

Small, C., & Sousa, D. (2016). Humans on Earth: Global extents of anthropogenic land cover from remote sensing. *Anthropocene*, *14*, 1–33. https://doi.org/10.1016/j.ancene.2016.04.003

Smith, M. O., Johnson, P. E., & Adams, J. B. (1985). Quantitative determination of mineral types and abundances from reflectance spectra using principal components analysis. *Journal of Geophysical Research*, *90*(S02), C797–C804. https://doi.org/10.1029/JB090iS02p0C797

Sousa, D., & Small, C. (2017). Global cross-calibration of Landsat spectral mixture models. *Remote Sensing of Environment*, *192*, 139–149. https://doi.org/10.1016/j.rse.2017.01.033

Spot Image (2002). SPOT satellite geometry handbook, S-NT-73-12-SI, Edition 1, Revision 0. Retrieved from http://www2.astrium-geo.com/files/pmedia/public/r439_9_spot_geometry_handbook.pdf

Stark, C. P., Barbour, J. R., Hayakawa, Y. S., Hattanji, T., Hovius, N., Chen, H., et al. (2010). The climatic signature of incised river meanders. *Science*, *327*(5972), 1497–1501. https://doi.org/10.1126/science.1184406

Tal, M., & Paola, C. (2010). Effects of vegetation on channel morphodynamics: Results and insights from laboratory experiments. *Earth Surface Processes and Landforms*, *35*(9), 1014–1028. https://doi.org/10.1002/esp.1908

Taramelli, A., & Barbour, J. (2006). A new DEM of Italy using SRTM data. *Italian Journal of Remote Sensing*, *36*, 3–15.

Taramelli, A., DiMatteo, L., Ciavola, P., Guadagnano, F., & Tolomei, C. (2014). Temporal evolution of patterns and processes of the coastal area in Bevano estuary (northern Adriatic) - Italy. *Ocean and Coastal Management*, *108*, 74–88. https://doi.org/10.1016/j.ocecoaman.2014.06.021

Taramelli, A., & Melelli, L. (2009). Map of deep seated gravitational slope deformation susceptibility in central Italy derived from SRTM DEM and spectral mixing analysis of the Landsat ETM+ data. *International Journal of Remote Sensing*, *30*(2), 357–387. https://doi.org/10.1080/01431160802339449

Taramelli, A., Pasqui, M., Barbour, J., Kirschbaum, D., Bottai, L., Busillo, C., et al. (2013). Spatial and temporal dust source variability in northern China identified using advanced remote sensing analysis. *Earth Surface Processes and Landforms*, *38*(8), 793–809. https://doi.org/10.1002/esp.3321

Taramelli, A., Reichenbach, P., & Ardizzone, F. (2008). Comparison of SRTM elevation data with cartographically derived DEMs in Italy. *Revista Geográfica Acadêmica*, *2*(viii), 41–52.

Taramelli, A., Valentini, E., & Cornacchia, L. (2015). Remote sensing solutions to monitor biotic and abiotic dynamics in coastal ecosystems. *Coastal Zones: Solutions for the 21st Century*, Chap.8, 125–135. https://doi.org/10.1016/B978-0-12-802748-6.00008-5

Taramelli, A., Valentini, E., Cornacchia, L., & Bozzeda, F. (2017). A hybrid power law approach for spatial and temporal pattern analysis of salt marsh evolution. *Journal of Coastal Research*, *77*, 63–73. https://doi.org/10.2112/SI77-007

Taramelli, A., Valentini, E., Cornacchia, L., Mandrone, S., Monbaliu, J., Thompson, R., et al. (2014). Modelling uncertainty in estuarine system by means of combined approach of optical and radar remote sensing, *Coastal Engineering 87*: 77–96. https://doi.org/10.1016/j.coastaleng.2013.11.001

Taramelli, A., Valentini, E., Innocenti, C., & Cappucci, S. (2013). FHYL: Field spectral libraries, airborne hyperspectral images and topographic and bathymetric LiDAR data for complex coastal mapping. *IEEE International on Geoscience and Remote Sensing Symposium (IGARSS)*, 2270–2273. https://doi.org/10.1109/IGARSS.2013.6723270

Temmerman, S., Bouma, T., Van de Koppel, J., Van der Wal, D., De Vries, M., & Herman, P. (2007). Vegetation causes channel erosion in a tidal landscape. *Geology*, *35*(7), 631–634. https://doi.org/10.1130/G23502A.1

Temmerman, S., Bouma, T. J., Govers, G., & Lauwaet, D. (2005). Flow paths of water and sediment in a tidal marsh: Relations with marsh developmental stage and tidal inundation height. *Estuaries*, *28*(3), 338–352. https://doi.org/10.1007/BF02693917

Thomson, A. G., Huiskes, A., Cox, R., Wadsworth, R. A., & Boorman, L. A. (2004). Short-term vegetation succession and erosion identified by airborne remote sensing of Westerschelde salt marshes, The Netherlands. *International Journal of Remote Sensing*, *25*(20), 4151–4176. https://doi.org/10.1080/01431160310001647688

Tiner, R. W. (2016). *Wetland indicators: A guide to wetland formation, identification, delineation, classification, and mapping*. Boca Raton, FL: CRC Press. https://doi.org/10.1201/9781315374710

Tolman, M. E., & Pranger, D. P. (2012). Toelichting bij de Vegetatiekartering Westerschelde 2010Rep., Rijkswaterstaat.

Valentini, E., Taramelli, A., Filipponi, F., & Giulio, S. (2014). An effective procedure for EUNIS and Natura 2000 habitat mapping in estuarine ecosystems integrating ecological knowledge and remote sensing analysis. *Ocean and Coastal Management*, *108*, 52–64.

Van Belzen J., (2011). Chess at the mud-flat. Using power-laws as indicator of salt-marsh ecosystem status and development. Master of Science thesis, Open University Netherlands.

van de Koppel, J., van der Wal, D., Bakker, J. P., & Herman, P. M. (2005). Self-organization and vegetation collapse in salt marsh ecosystems. *The American Naturalist*, *165*(1), E1–E12. https://doi.org/10.1086/426602

van Wesenbeeck, B. K., Van De Koppel, J., Herman, P. M. J., & Bouma, T. J. (2008). Does scale-dependent feedback explain spatial complexity in salt-marsh ecosystems? *Oikos*, *117*(1), 152–159. https://doi.org/10.1111/j.2007.0030-1299.16245.x

Vande Castle, J. (1998). Remote sensing applications in ecosystem analysis. In D. L. Peterson & V. T. Parker (Eds.), *Ecological scale theory and applications* (pp. 271–287). New York: Columbia University Press.

Vandenbruwaene, W., Bouma, T. J., Meire, P., & Temmerman, S. (2012). Bio-geomorphic effects on tidal channel evolution: Impact of vegetation establishment and tidal prism change. *Earth Surface Processes and Landforms*, *38*(2), 122–132.

Vandenbruwaene, W., Temmerman, S., Bouma, T. J., Klaassen, P., De Vries, M., Callaghan, D., et al. (2011). Flow interaction with dynamic vegetation patches: Implications for biogeomorphic evolution of a tidal landscape. *Journal of Geophysical Research*, *116*, F01008. https://doi.org/10.1029/2010JF001788

Wang, C., Menenti, M., Stoll, M. P., Belluco, E., & Marani, M. (2007). Mapping mixed vegetation communities in salt marshes using airborne spectral data. *Remote Sensing of Environment*, *107*(4), 559–570. https://doi.org/10.1016/j.rse.2006.10.007

Wang, C., & Temmerman, S. (2013). Does biogeomorphic feedback lead to abrupt shifts between alternative landscape states?: An empirical study on intertidal flats and marshes. *Journal of Geophysical Research: Earth Surface*, *118*, 229–240. https://doi.org/10.1029/2012JF002474

Weerman, E. J., Herman, P. M. J., & van de Koppel, J. (2010). Top-down control inhibits spatial self-organization of a patterned landscape). *The American Naturalist*, *176*(1), E15–E32. https://doi.org/10.1086/652991

Weerman, E. J., van Belzen, J., Rietkerk, M., Temmerman, S., Kefi, S., Herman, P. M. J., & van de Koppel, J. (2012). Changes in diatom patch-size distribution and degradation in a spatially self-organized inter tidal mudflat ecosystem. *Ecology*, *93*(3), 608–618. https://doi.org/10.1890/11-0625.1

Yapp, R. H., Johns, D., & Jones, O. T. (1916). The salt marshes of the Dovey estuary: Part I. Introductory. *Journal of Ecology*, *4*(1), 27–42. https://doi.org/10.2307/2255448

Yapp, R. H., Johns, D., & Jones, O. T. (1917). The salt marshes of the Dovey estuary: Part II. The salt marshes. *Journal of Ecology*, *5*, 65–103.